



ELSEVIER

Available online at [www.sciencedirect.com](http://www.sciencedirect.com)

SCIENCE @ DIRECT®

Proceedings of the Combustion Institute 30 (2005) 285–293

Proceedings  
of the  
Combustion  
Institute

[www.elsevier.com/locate/proci](http://www.elsevier.com/locate/proci)

# Lean or ultra-lean stretched planar methane/air flames

Zhongxian Cheng\*, Joseph A. Wehrmeyer, Robert W. Pitz

*Mechanical Engineering Department, Vanderbilt University, Box 1592 Station B, Nashville, TN 37235, USA*

## Abstract

Lean premixed combustion has potential advantages of reducing pollutants and improving fuel economy. In some lean engine concepts, the fuel is directly injected into the combustion chamber resulting in a distribution of lean fuel/air mixtures. In this case, very lean mixtures can burn when supported by hot products from more strongly burning flames. This study examines the downstream interaction of opposed jets of a lean-limit CH<sub>4</sub>/air mixture vs. a lean H<sub>2</sub>/air flame. The CH<sub>4</sub> mixtures are near or below the lean flammability limit. The flame composition is measured by laser-induced Raman scattering and is compared to numerical simulations with detailed chemistry and molecular transport including the Soret effect. Several sub-limit lean CH<sub>4</sub>/air flames supported by the products from the lean H<sub>2</sub>/air flame are studied, and a small amount of CO<sub>2</sub> product (around 1% mole fraction) is formed in a “negative flame speed” flame where the weak CH<sub>4</sub>/air mixture diffuses across the stagnation plane into the hot products from the H<sub>2</sub>/air flame. Raman scattering measurements of temperature and species concentration are compared to detailed simulations using GRI-3.0, C<sub>1</sub>, and C<sub>2</sub> chemical kinetic mechanisms, with good agreement obtained in the lean-limit or sub-limit flames. Stronger self-propagating CH<sub>4</sub>/air mixtures result in a much higher concentration of product (around 6% CO<sub>2</sub> mole fraction), and the simulation results are sensitive to the specific chemical mechanism. These model-data comparisons for stronger CH<sub>4</sub>/air flames improve when using either the C<sub>2</sub> or the Williams mechanisms.

© 2004 The Combustion Institute. Published by Elsevier Inc. All rights reserved.

*Keywords:* Hot products; Ultra-lean; Sub-limit; Counterflow flames; Raman scattering

## 1. Introduction

Lean combustion is currently under investigation due to its potential advantages in limiting thermal NO<sub>x</sub> emissions and in reducing fuel consumption. It has been used in gas turbines and direct injection spark ignition (DISI) engines. But a critical problem is that lean combustion tends to produce unburned hydrocarbon pollutants. For example, in DISI engines, ultra-lean combustion

is achieved by charge stratification. The fuel/air mixture is inhomogeneous, leading to the simultaneous formation of lean, rich, and stoichiometric regions. For the inhomogeneous reactants, Haworth et al. [1] simulated turbulent inhomogeneous combustion in DISI engines and found that hydrocarbon-rich fragments and oxidizer penetrate behind the primary heat-release zone to form a secondary reaction zone. Flames occurring in an inhomogeneously mixed fuel and air region are examples of partially premixed combustion. Some of this partially premixed mixture is so lean that it does not burn. But this ultra-lean mixture may still react if hot products interact with it. That is, under certain conditions, the lean

\* Corresponding author. Fax: +1 615 343 6687.

E-mail address: [zhongxian.cheng@vanderbilt.edu](mailto:zhongxian.cheng@vanderbilt.edu) (Z. Cheng).

mixture region can burn and thus reduce the potential pollutants. The interaction of lean mixture with hot products needed to maintain the lean region burning is the focus of this work.

Partially premixed flames have been studied widely. In particular, the downstream interaction between two premixed streams was investigated by Sohrab et al. [2]. Most practical flames are stretched. The stretch effect combined with other aspects such as the effect of Lewis number or curvature will modify flame structure significantly [3,4]. Considering the various conditions that exist simultaneously in inhomogeneous fuel/air reaction, a set of CH<sub>4</sub>/air flames with a wide range of equivalence ratios and stretch rates impinging upon hot products are studied experimentally and numerically. The opposed jet burner generates counterflow flames that are widely used to study chemical kinetics and species transport under aerodynamic stretch. Using the opposed jet flames, partially premixed CH<sub>4</sub>/air vs. air flame structures were investigated [5,6]. Lean partially premixed CH<sub>4</sub> and C<sub>3</sub>H<sub>8</sub> flame structures vs. hot products have also been investigated [7,8]. In general, premixed flames [9,10] are much less sensitive to stretch than diffusion flames [11]. In the present work, stretch effects on the flame structure of the interaction between hot products and lean CH<sub>4</sub>/air mixtures are studied with Raman scattering and detailed transport, complex chemistry numerical simulations.

## 2. Experimental system and flames examined

Measurement of major species and temperature are made along the centerline of an opposed jet burner using a non-intrusive Raman diagnostic system. The Raman system is the same as used previously and the details are given in [4,8]. Number density measurements of major species are directly related to their spontaneous Raman signal strengths, and since all major species are measured, the total number density of the local gas mixture is obtained and related to temperature via the ideal gas law (assuming pressure is 1 atm). For the present work, the opposed jet burner has been modified by inserting honeycomb metal “flow straighteners” into both nozzles. These inserts have 0.8 mm honeycomb cells that are 19 mm in length. The inserts provide a very uniform exit velocity profile for both the nozzles, as verified by hot wire anemometry traverses in non-reacting flow. In addition the new honeycomb metal inserts do not cause flame attachment of either H<sub>2</sub>/air or hydrocarbon/air flames. The opposed jet burner was designed by Seshadri et al. [12] and has been used extensively for hydrogen- and hydrocarbon-fueled diffusion flames and for hydrocarbon-fueled premixed flames. With the honeycomb inserts, rather than wire screens,

it can also be used for lean H<sub>2</sub>/air premixed flames.

Eight flames, which are classified into three groups, are investigated by experiment and numerical simulation. All three groups have 300 K inlet conditions for both jets. Group A includes three flames of CH<sub>4</sub>/air mixtures, all with an equivalence ratio 0.68, vs. lean H<sub>2</sub>/air mixtures at stretch rates of 90, 140, and 210 s<sup>-1</sup>. Group B includes three flames of CH<sub>4</sub>/air mixtures, all with  $\phi$  of 0.54, vs. lean H<sub>2</sub>/air mixtures at stretch rates 90, 140, and 210 s<sup>-1</sup>. Group C includes two ultra-lean sub-limit flames of CH<sub>4</sub>/air mixtures ( $\phi = 0.33$  or 0.43) vs. lean H<sub>2</sub>/air mixtures at a stretch rate 140 s<sup>-1</sup>. The maximum Reynolds number of jet flow is 1600 at a stretch rate 210 s<sup>-1</sup>. All of the lean H<sub>2</sub>/air mixtures have the same  $\phi$  of 0.28 and the calculated OH, O, and H mole fractions for the H<sub>2</sub>/air flames are of the order of  $1 \times 10^{-3}$ ,  $8 \times 10^{-4}$ , and  $5 \times 10^{-4}$ , respectively. This equivalence ratio is chosen to cause the lean H<sub>2</sub>/air flame to be detached from the exit of the burner but still be separated from the CH<sub>4</sub>/air flame. CH<sub>4</sub> is a good alternate fuel because of its well-known chemical kinetics. Similar work has already been performed for planar C<sub>3</sub>H<sub>8</sub>/air flames vs. hot products, but problems were encountered with the opposed jet burner used at the time [7]. Because premixed H<sub>2</sub>/air has a fast burning velocity and tends to attach to the mesh screen or sintered metal plate at the nozzle exit (used to provide a top hat velocity profile), the boundary conditions were not well established [7]. Here, a lean H<sub>2</sub>/air flame with well-established boundary conditions is used to generate hot products so that only high temperature water vapor, O<sub>2</sub>, and N<sub>2</sub> impinge upon the hydrocarbon flame. Thus, any CO<sub>2</sub> formed must come from the downstream interaction of the methane fuel and the hot products. The CO<sub>2</sub> is an indicator of the amount of CH<sub>4</sub> fuel that is burned.

## 3. Numerical simulations and mechanisms

Numerical flame simulation is performed with “OPPDIF” [13]. Detailed chemical kinetic mechanisms and transport data are used for numerical predictions. Four different chemical kinetic mechanisms are used for methane flames: one which models hydrocarbons with only one carbon atom (C<sub>1</sub>) [14], one which models hydrocarbons containing up to two carbon atoms (C<sub>2</sub>) [14], GRI-3.0 [15], and Williams et al. [16].

## 4. Results and discussion

Experimental results from the Raman scattering measurement are achieved based on relevant calibration curves obtained across a wide equivalence

lence ratio range from  $\text{H}_2/\text{air}$ ,  $\text{H}_2/\text{CO}/\text{air}$ , and  $\text{H}_2/\text{CO}_2/\text{air}$  flames above a 25 mm diameter Hencken calibration burner, where chemical equilibrium is assumed at some distance downstream of the burner surface. Each opposed jet flame is modeled with the four detailed chemical kinetic mechanisms. Comparisons between experimental results and numerical simulation are performed for each flame.

Figure 1 shows a set of Raman spectral graphs from the flame:  $\text{CH}_4/\text{air}$  ( $\phi = 0.68$ ) vs.  $\text{H}_2/\text{air}$  ( $\phi = 0.28$ ). They are two representative spectra from different locations along the centerline of the opposed jet burner. Each spectrum is the result of a 600 laser pulse accumulation of light signals onto the CCD, and each spectrum has background luminosity subtracted. It is found that all laser-induced background levels are very low for the lean premixed flames examined. The spatial resolution of the Raman measurement is 0.2 mm [8]. CO signals are detected in the flames but with too much uncertainty to be quantified.

At a given temperature and pressure, the flammability limit defines the equivalence ratio regime beyond which no flame will propagate. The lean flammability limits of  $\text{CH}_4/\text{air}$  and  $\text{H}_2/\text{air}$  mixture are 5% (fuel mole fraction) or  $\phi$  of 0.5 and 4% or  $\phi$  of 0.10, respectively [17]. By definition, the flammability limit is independent of external parameters [3]. The determination of flammability limit should be based on a stretchless adiabatic flame.

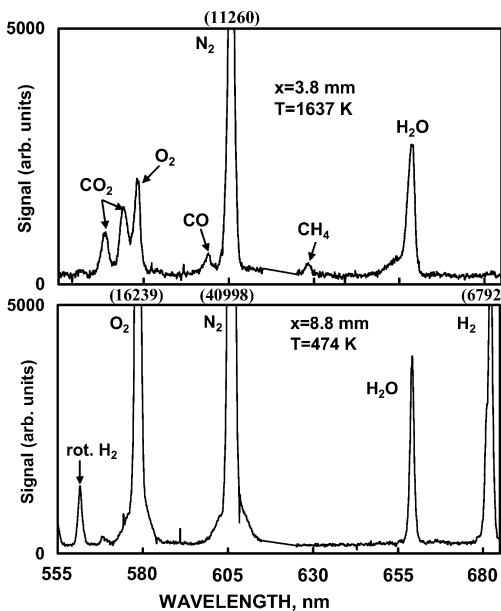


Fig. 1. Representative Raman spectra obtained from the flame shown in Fig. 2. Spectra correspond to two axial positions along the centerline of the opposed jet burner where “ $x$ ” is the distance from the top jet.

Usually, the limit is determined from the stretched flame data extrapolated to zero stretch rate [3], although this approach is disputed by Ju et al. [18]. All flames studied in this work are stretched premixed flames and their extinction limits depend on the mixture equivalence ratio, stretch rate, preferential diffusion (Lewis number effect), and heat loss.

#### 4.1. Group A: stretched $\text{CH}_4/\text{air}$ mixture with $\phi = 0.68$ vs. hot products

For  $\phi = 0.68$ , the  $\text{CH}_4/\text{air}$  mixture is above the lean flammability limit and forms a self-propagating flame at low stretch rate because of its sufficient strength. The aerodynamic stretch rate varies from  $90 \text{ s}^{-1}$  to near an extinction limit,  $210 \text{ s}^{-1}$ . When the stretch rate is below some stretch rate (e.g.,  $140 \text{ s}^{-1}$ ), the flames are relatively strong. Such a flame structure is shown in Fig. 2. Near the extinction condition ( $\kappa = 210 \text{ s}^{-1}$ ), the flames become very weak and almost invisible, even though the equivalence ratio is still 0.68. The flame structure is given in Fig. 4.

Experimental measurements and numerical predictions of temperature and reactant concentrations are compared in Fig. 2 for the methane/air ( $\phi = 0.68$ ) mixture vs. hot products at stretch rate  $\kappa = 140 \text{ s}^{-1}$ . The dashed line indicates the stagnation plane from modeling where the axial velocity is zero. As seen from the experimental data, a premixed “positive flame speed” flame exists on the  $\text{CH}_4/\text{air}$  side of the stagnation plane [2]. The uncertainties caused by shot noise are negligible and overall uncertainty for various species and temperature is about 3%. The representative error bars are shown in Fig. 2. The results shown in Fig. 2 are from the Williams mechanism. The flame

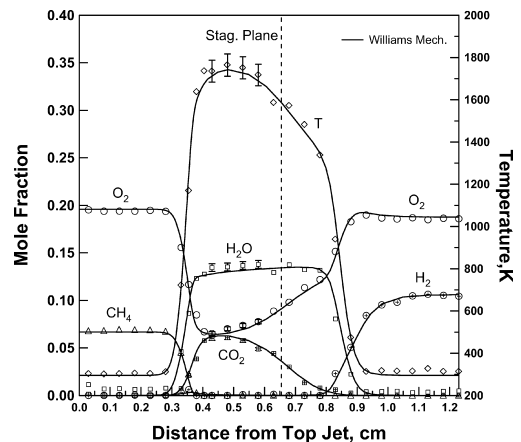


Fig. 2. Experimental and numerically predicted species and temperature profiles for:  $\text{CH}_4/\text{air}$  ( $\phi = 0.68$ ) vs.  $\text{H}_2/\text{air}$  ( $\phi = 0.28$ ),  $\kappa = 140 \text{ s}^{-1}$ .

location is determined by fresh reactants velocity and local laminar flame speed. For a particular equivalence ratio (i.e.,  $\phi = 0.68$ ), the laminar flame speed almost does not change vs. stretch, so for higher reactant velocity indicated by higher stretch rate, the closer the flame location is to the stagnation plane. It is found that experimental profiles of all the major species and temperature match very well to the numerically predicted profiles by the Williams and the  $C_2$  mechanisms. The  $CH_4$ /air flame is located about 3.5 mm away from the top jet, and the lean  $H_2$ /air flame is located downstream 8 mm from the top jet. The stagnation plane is located near the middle of the two jet exits. The peak flame temperature is close to 1800 K. About 6%  $CO_2$  mole fraction is formed in the postflame zone. Further it is found that the peak temperature and the peak  $CO_2$  concentration are not strongly influenced by the change in stretch rate  $\kappa$ .

Numerical predictions are performed with the four different chemical mechanisms and are shown in Fig. 3. From Fig. 3 on the  $CH_4$ /air flame side, the Williams and the  $C_2$  mechanisms demonstrate a relatively fast flame speed; the  $C_1$  mechanism predicts a slightly lower flame speed. The GRI-3.0 mechanism gives an intermediate flame speed. But on the lean  $H_2$ /air flame side, there is almost no difference in the laminar flame speed. As seen in Figs. 2 and 3, the Williams mechanism or the  $C_2$  mechanism give the best agreement with experimental data when the stretch rate  $\kappa$  is below  $140 \text{ s}^{-1}$  for  $\phi = 0.68$ .

The flame structure near extinction ( $\kappa = 210 \text{ s}^{-1}$ ) is given by Fig. 4. Although modeling results using the four mechanisms (numerical results in Fig. 4 use the Williams mechanism) show the flame temperature only drops slightly due to the high stretch rate, the experimental data show a completely different flame structure; the

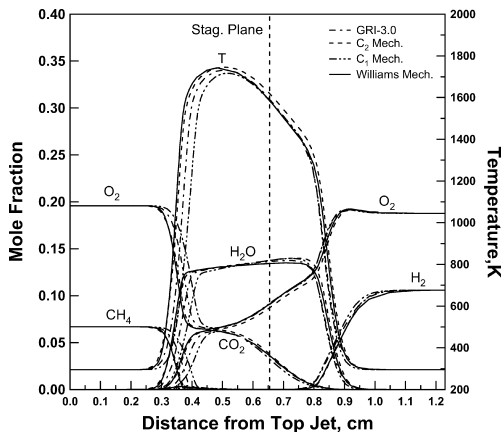


Fig. 3. Numerically predicted species and temperature profiles using four different mechanisms for:  $CH_4$ /air ( $\phi = 0.68$ ) vs.  $H_2$ /air ( $\phi = 0.28$ ),  $\kappa = 140 \text{ s}^{-1}$ .

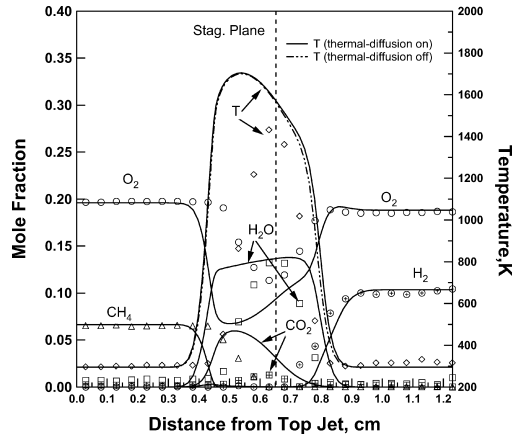


Fig. 4. Experimental and numerically predicted species and temperature profiles for:  $CH_4$ /air ( $\phi = 0.68$ ) vs.  $H_2$ /air ( $\phi = 0.28$ ),  $\kappa = 210 \text{ s}^{-1}$ . Numerical simulation uses the Williams mechanism.

strong self-propagating flame is not formed at that high stretch rate. It is clear that none of the four mechanisms is appropriate for this lean, near-extinction flame. There is a big discrepancy because the numerical results indicate a premixed flame, but actually the flame is near extinction. Therefore, the flame speed and peak temperature from experimental data are far lower than the predicted values. The actual observed flame is a so-called “negative flame speed flame” [2,3,19] because of its formation by  $CH_4$  fuel diffusing across the stagnation plane and reacting with the hot products from the lean  $H_2$ /air premixed flame at the other jet.

For a lean  $CH_4$ /air mixture at room temperature, the thermal diffusivity coefficient is  $0.213 \text{ cm}^2/\text{s}$  and mass diffusivity (methane in air) is  $0.220 \text{ cm}^2/\text{s}$ . Thus, the Lewis number (the ratio of thermal diffusivity to mass diffusivity) is 0.97 and is very close to unity. Therefore, the lean  $CH_4$ /air mixture has an approximately neutral preferential diffusivity, and the stretch rate will not affect the flame structure or flame speed too much [3,9,10]. This is true for  $\kappa = 90 \text{ s}^{-1}$  and  $\kappa = 140 \text{ s}^{-1}$  flames (not shown), even though peak temperature still decreases about 40 K when stretch rate changes from 90 to  $140 \text{ s}^{-1}$ . In these cases, the premixed flame is not located near the stagnation plane and can adjust its location to match the changed inlet jet velocity.

Figure 4 also shows the thermal-diffusion effect (Soret effect) on flame temperature profile ( $\kappa = 210 \text{ s}^{-1}$ , using the Williams mechanism). The numerical simulation is done by turning on and off the Soret effect. On the lean  $CH_4$ /air flame side, temperature profiles are the same with and without the Soret, but they are slightly different on the lean  $H_2$ /air flame side at the higher stretch

rate. The temperature gradient on the lean H<sub>2</sub>/air flame side contributes to the mass diffusion velocities due to the small molecular weight of the H<sub>2</sub> fuel.

4.2. Group B: stretched CH<sub>4</sub>/air mixture with  $\phi = 0.54$  vs. hot products

The equivalence ratio for the CH<sub>4</sub>/air flames shown in Figs. 5–7 is  $\phi = 0.54$  that is near the flammability limit,  $\phi = 0.50$ . Again, the aerodynamic stretch rate varies from 90 s<sup>-1</sup> to near extinction 210 s<sup>-1</sup>. Contrary to the  $\phi = 0.68$  flames, lean CH<sub>4</sub>/air premixed self-propagating flames do not exist on the CH<sub>4</sub>/air side of the stagnation plane for each stretch rate condition for the

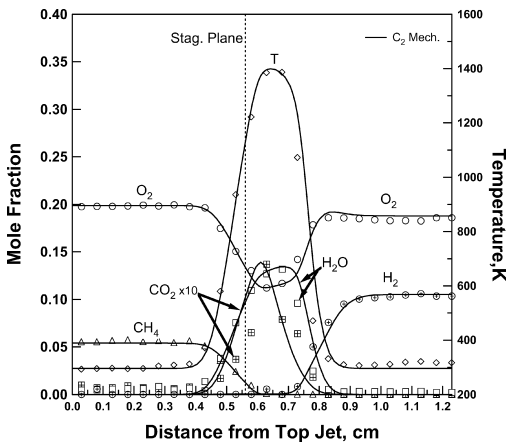


Fig. 5. Experimental and numerically predicted species and temperature profiles for: CH<sub>4</sub>/air ( $\phi = 0.54$ ) vs. H<sub>2</sub>/air ( $\phi = 0.28$ ),  $\kappa = 140$  s<sup>-1</sup>.

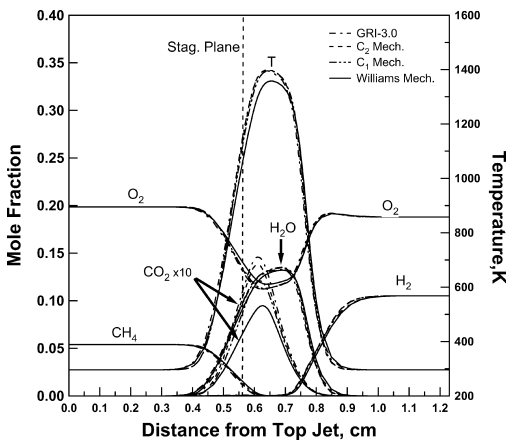


Fig. 6. The comparison of numerically predicted species and temperature profiles using four different mechanisms for: CH<sub>4</sub>/air ( $\phi = 0.54$ ) vs. H<sub>2</sub>/air ( $\phi = 0.28$ ),  $\kappa = 140$  s<sup>-1</sup>.

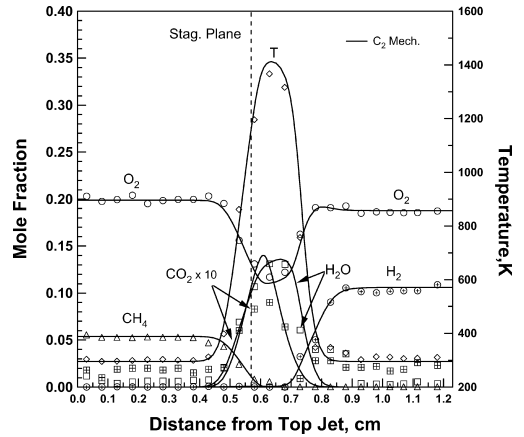


Fig. 7. Experimental and numerically predicted species and temperature profiles for: CH<sub>4</sub>/air ( $\phi = 0.54$ ) vs. H<sub>2</sub>/air ( $\phi = 0.28$ ),  $\kappa = 210$  s<sup>-1</sup>.

$\phi = 0.54$  CH<sub>4</sub>/air mixture. Instead very weak “negative flame speed” flames are formed by CH<sub>4</sub> diffusing across the stagnation plane and reacting with the excess O<sub>2</sub> from the H<sub>2</sub>/air premixed flame from the other jet [2,3,19]. This weak flame is located at the peak of the CO<sub>2</sub> profile.

The detailed flame structure for the stretch rate  $\kappa = 140$  s<sup>-1</sup> condition is shown in Fig. 5. Experimental measurements and numerical predictions of temperature and reactant concentrations are compared. Compared to the flame at  $\kappa = 90$  s<sup>-1</sup> (not shown), the CH<sub>4</sub>/air flame is closer to the H<sub>2</sub>/air flame at  $\kappa = 140$  s<sup>-1</sup>. There is excellent agreement in the model-data comparison when using the C<sub>2</sub> mechanism. The peak temperature, peak CO<sub>2</sub>, and peak H<sub>2</sub>O are located on the H<sub>2</sub>/air flame side. The O<sub>2</sub> profile is interesting, as there is a local “bump” close to the H<sub>2</sub>/air flame, but on the CH<sub>4</sub>/air mixture side, the O<sub>2</sub> profile is very smooth. This is due to non-equidiffusion for the H<sub>2</sub>/air mixture causing local “strengthening” of the flame. The comparison for different mechanisms is given in Fig. 6 for the same flame. For clarity, the experimental data are not shown. The predictions for T, O<sub>2</sub>, CO<sub>2</sub>, CH<sub>4</sub>, and H<sub>2</sub>O based on the GRI-3.0, C<sub>1</sub>, and C<sub>2</sub> mechanisms are almost the same (CO<sub>2</sub> is magnified by 10 times for good identification). The predictions based on the Williams mechanism are obviously different with that from the GRI-3.0, C<sub>1</sub>, and C<sub>2</sub> mechanisms. The predicted temperature is about 40 K lower, and CO<sub>2</sub> peak mole fraction is lower by a mole fraction value of 0.6%. In Fig. 3, predictions with the Williams mechanism show a stronger flame structure than other mechanisms. But for this very lean diffusion dominated flame, predictions with the Williams mechanism give the opposite trend.

The flame structure for  $\kappa = 210$  s<sup>-1</sup> in Fig. 7 shows good agreement with the C<sub>2</sub> mechanism (simulation using the GRI-3.0 mechanism gives

similar results, not shown). The flame itself is very similar to that for  $\kappa = 140 \text{ s}^{-1}$ , except the reaction zone is narrower. For the diffusion flame, the flame thickness inversely scales with  $\kappa^{1/2}$  [11]. Here, the flame is not a pure diffusion flame, but is a “negative flame speed”  $\text{CH}_4/\text{air}$  diffusion flame formed by diffusion of a lean  $\text{CH}_4/\text{air}$  mixture into the hot products from the lean  $\text{H}_2/\text{air}$  flame. But the trend is still true for this case, that is, the flame reaction zone is becoming narrower with increasing stretch rate. Incomplete reaction caused by higher stretch rate leads to lower temperature and eventual mutual flame extinction even though hot products from the lean  $\text{H}_2/\text{air}$  flame interacting downstream can extend this extinction up to a much higher level.

#### 4.3. Group C: stretched sub-limit $\text{CH}_4/\text{air}$ mixture vs. hot products

The lean limit for  $\text{CH}_4/\text{air}$  mixture is 5% (volume) or  $\phi = 0.50$ . Based on the definition of flammability limit, the mixtures of  $\phi = 0.33$  and  $0.43$  studied in Figs. 8 and 9 are too lean under this limit to burn at any condition. However, Ju et al. [18,20] numerically studied the sub-limit combustion at varied stretch rate and found that some sub-limits exist. Here, our planar flame experiment shows that extinction limit is dependent on external conditions such as preferential diffusion, stretch rate, and support of hot products. For the  $\text{CH}_4/\text{air}$  flame, the mixture limits can go to as low of an equivalence ratio as  $\phi = 0.16$  if downstream hot products support the flame, even though the visible flame is very weak. Hot products commonly exist in turbulent combustion such as in combustors stabilized by recirculation zones. So, this indicates the potential of sub-limit lean combustion supported by hot products.

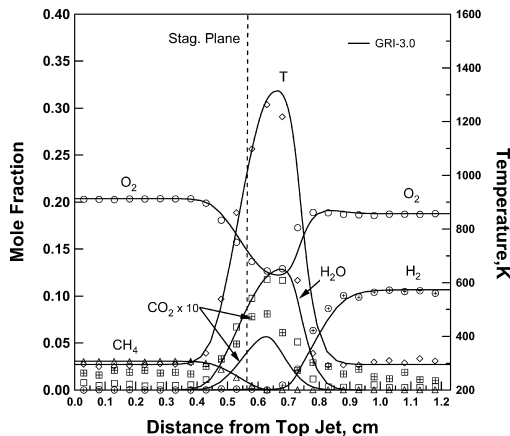


Fig. 8. Experimental and numerically predicted species and temperature profiles for:  $\text{CH}_4/\text{air}$  ( $\phi = 0.33$ ) vs.  $\text{H}_2/\text{air}$  ( $\phi = 0.28$ ),  $\kappa = 140 \text{ s}^{-1}$ .

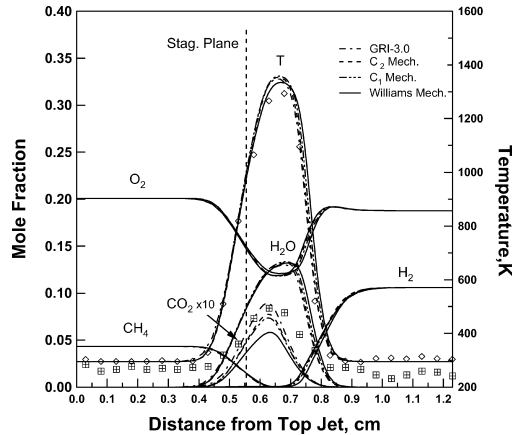


Fig. 9. The comparison of numerically predicted species and temperature profiles using four mechanisms for:  $\text{CH}_4/\text{air}$  ( $\phi = 0.43$ ) vs.  $\text{H}_2/\text{air}$  ( $\phi = 0.28$ ),  $\kappa = 140 \text{ s}^{-1}$ . Experimental data for  $\text{CO}_2$  and temperature are shown.

Figure 8 shows the sub-limit flame structure of a  $\text{CH}_4/\text{air}$  mixture ( $\phi = 0.33$ ) vs.  $\text{H}_2/\text{air}$  ( $\phi = 0.28$ ) mixture ( $\kappa = 140 \text{ s}^{-1}$ ). This is a very weak negative flame speed flame. The flame temperature drops to 1300 K, just above the ignition temperature. Predictions based on the GRI-3.0 mechanism (simulation using the  $\text{C}_2$  mechanism indicates no reaction) give good agreement with experiment data for reactants and temperature. The measured  $\text{CO}_2$  is 40% higher than predicted. Due to the low  $\text{CO}_2$  concentration, there is some noise and uncertainty, and it is not clear if the discrepancy comes from the modeling itself or experimental uncertainty. The  $\text{CO}_2$  mole fraction of  $\sim 0.6\%$  (6000 ppm) is close to the Raman detection limit.

Another sub-limit flame structure of  $\text{CH}_4/\text{air}$  ( $\phi = 0.43$ ) vs.  $\text{H}_2/\text{air}$  ( $\phi = 0.28$ ) is shown in Fig. 9. To compare the effect of the specific chemical mechanism on this sub-limit flame structure, predicted flame structures based on four different mechanisms are given (experimental data for  $\text{CO}_2$  and temperature are shown). Again the  $\text{C}_1$ ,  $\text{C}_2$ , and GRI-3.0 mechanisms give very similar predictions for this diffusion controlled “negative flame speed” flame. Consistent with other weak flames (Fig. 6), the Williams mechanism predicted a slightly weaker flame structure as indicated by a lower predicted peak temperature and lower predicted peak  $\text{CO}_2$  mole fraction.

#### 4.4. Stretch effect on $\text{CO}_2$ concentration and temperature

Figure 10 shows the effect of stretch on peak  $\text{CO}_2$  concentration and peak temperature for flames with equivalence ratios of  $\phi = 0.68$  and  $0.54$ . For equivalence ratio 0.68 flames in Fig. 10, the numerical simulation implies that there is no obvious delimit for positive self-propagating flame

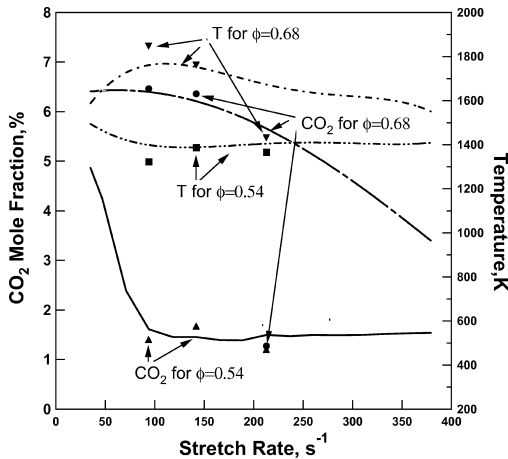


Fig. 10. Experimental and numerically predicted  $\text{CO}_2$  peak concentration and peak temperature at various stretch rate for:  $\text{CH}_4/\text{air}$  ( $\phi = 0.54$  or  $0.68$ ) vs.  $\text{H}_2/\text{air}$  ( $\phi = 0.28$ ),  $\kappa = 140 \text{ s}^{-1}$ . Numerical simulation uses GRI-3.0.

to negative flame speed diffusion flame. When stretch rate increases, the temperature and  $\text{CO}_2$  peak mole fraction drops smoothly. But the experimental data show that the flame is very weak at a stretch rate of  $210 \text{ s}^{-1}$  and the flame becomes a “negative flame speed” flame. The modeling does not predict the sudden drop in temperature and  $\text{CO}_2$  that indicates a “negative flame speed” flame. For equivalence ratio  $\phi = 0.54$  flames, the numerical simulation implies that it is a self-propagating premixed flame at very low stretch rate ( $< 50 \text{ s}^{-1}$ ). Although no experimental data could be obtained at this low stretch rate, it is conceivable that a positive flame speed flame can exist at the low stretch rate. When increasing stretch rate, both experimental data and predictions indicate the existence of a “negative flame speed” flame instead of the self-propagating premixed flame. There is a large drop in the  $\text{CO}_2$  concentration at  $\kappa = 100 \text{ s}^{-1}$ . An interesting result is that the  $\text{CO}_2$  concentration is constant ( $\sim 1\%$ ) when the stretch rate is increased which means the flame strength is unchanged. The trend for temperature change with stretch is also shown in Fig. 10.

Comparison of the temperature profiles for various equivalence ratios of  $\text{CH}_4/\text{air}$  vs. lean  $\text{H}_2/\text{air}$  ( $\phi = 0.28$ ) at  $\kappa = 140 \text{ s}^{-1}$  is shown in Fig. 11. The GRI-3.0 mechanism gives a good prediction over the whole range. This clearly shows changes of the flame temperature and flame structure when changing equivalence ratio. That is, equivalence ratios 0.54 or below shows the “negative flame speed” diffusion flame formed by interaction with the hot products. When mixture equivalence ratio goes above 0.68, self-propagating flames are formed and the hot products from the  $\text{H}_2/\text{air}$  flame have little influence.

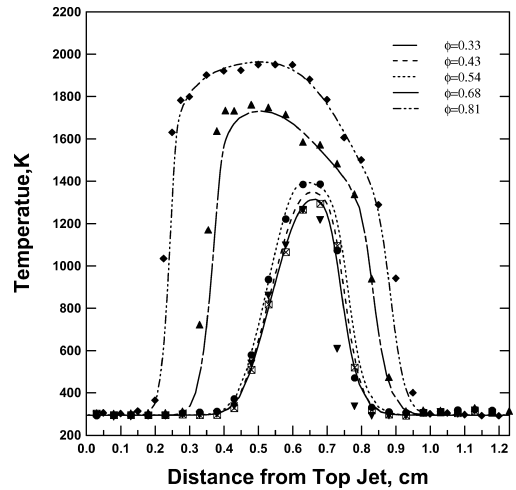


Fig. 11. Experimental and numerically predicted temperature profiles for different equivalence ratio of  $\text{CH}_4/\text{air}$  vs.  $\text{H}_2/\text{air}$  ( $\phi = 0.28$ ),  $\kappa = 140 \text{ s}^{-1}$ . Numerical simulation uses GRI-3.0.

## 5. Summary

The flame structures of lean premixed planar  $\text{CH}_4/\text{air}$  flames, opposed by hot products produced by a lean  $\text{H}_2/\text{air}$  flame, are investigated by experiment and numerical simulation. A diffusion controlled “negative flame speed” flame exists when the premixed  $\text{CH}_4$  mixture is very lean and it has to burn with the support from external hot products. With the support of these hot products, the lean flammability limit can be extended to a very lean range, allowing sub-limit combustion. Ultra-lean  $\text{CH}_4/\text{air}$  flames ( $\phi = 0.33, 0.43$ ), which are below the flammability limit ( $\phi = 0.5$ ), are studied. Predictions with the GRI-3.0 mechanism show good agreement for most species concentration and temperature measurement even though there is some discrepancy in the  $\text{CO}_2$  profile for the two sub-limit flames. The  $\text{CO}_2$  peak mole fraction is approximately 1% for these ultra-lean flames. Predictions of  $\text{CO}_2$  profiles based on the Williams mechanism are substantially lower than those by the GRI-3.0 mechanism.

Lean  $\text{CH}_4/\text{air}$  ( $\phi = 0.54$ ) flames, above the flammability limit ( $\phi = 0.5$ ), supported by hot products show the downstream interaction supports a very weak diffusion flame by supplying high temperature products or flame radicals. From low stretch rate to near extinction, numerical simulations with the  $\text{C}_2$ ,  $\text{C}_1$ , and GRI-3.0 mechanisms show good agreement with experimental data. Simulation with the Williams mechanism predicts a slightly low  $\text{CO}_2$  peak compared to other mechanisms. But there is an opposite trend for self-propagating flames with equivalence ratio of 0.68. Lean  $\text{CH}_4/\text{air}$

( $\phi = 0.68$ ) flames supported by hot products show very good agreement between experimental data and numerical results when the stretch rate is below  $140 \text{ s}^{-1}$ . The Williams mechanism and the  $\text{C}_2$  mechanism give better predictions than the  $\text{C}_1$  or GRI-3.0 mechanism. The Williams mechanism predicts a higher flame speed and gives the best agreement with the experiment data for self-propagating, low stretch rate flames at  $\phi = 0.68$   $\text{CH}_4/\text{air}$  mixtures. But when the stretch rate is increased to  $210 \text{ s}^{-1}$ , the observed flame structure is completely different from that predicted by all four mechanisms. The simulations predict a self-propagating flame and the experiment shows a “negative flame speed” flame.

### Acknowledgments

This work is partly supported by the US Department of Energy’s Office of Basic Energy Sciences, Partnerships for Academic-Industrial Research (PAIR) Grant (No. DE-FG02-98ER14915), with Dr. Alan H. Laufer as the technical monitor.

### References

- [1] D.C. Haworth, R.J. Blint, B. Cuenot, T.J. Poinot, *Combust. Flame* 121 (3) (2000) 395–417.
- [2] S.H. Sohrab, Z.Y. Ye, C.K. Law, *Proc. Combust. Inst.* 20 (1984) 1957–1965.
- [3] C.K. Law, *Proc. Combust. Inst.* 22 (1988) 1381–1402.
- [4] D.M. Mosbacher, J.A. Wehrmeyer, R.W. Pitz, C.J. Sung, J.L. Byrd, *Proc. Combust. Inst.* 29 (2002) 1479–1486.
- [5] M.A. Tanoff, M.D. Smooke, R.J. Osborne, T.M. Brown, R.W. Pitz, *Proc. Combust. Inst.* 26 (1996) 1121–1128.
- [6] R.S. Barlow, A.N. Karpetis, J.H. Frank, J.-Y. Chen, *Combust. Flame* 127 (2001) 2102–2118.
- [7] J.A. Wehrmeyer, Z. Cheng, D.M. Mosbacher, R.W. Pitz, R. Osborne, *Combust. Flame* 128 (3) (2002) 232–241.
- [8] Z. Cheng, J.A. Wehrmeyer, and R.W. Pitz, in: *38th AIAA/ASME/SAE/ASEE Joint Propulsion Conference, AIAA 2002-4021*. Indianapolis, IN, 2002.
- [9] C.J. Sung, J.B. Liu, C.K. Law, *Combust. Flame* 106 (1-2) (1996) 168–183.
- [10] C.K. Law, C.J. Sung, G. Yu, R.L. Axelbaum, *Combust. Flame* 98 (1-2) (1994) 139–154.
- [11] C.J. Sung, J.B. Liu, C.K. Law, *Combust. Flame* 102 (4) (1995) 481–492.
- [12] K. Seshadri, I. Puri, N. Peters, *Combust. Flame* 61 (3) (1985) 237–249.
- [13] R.J. Kee, F.M. Rupey, J.A. Miller, M.E. Coltrin, J.F. Grcar, E. Meeks, H.K. Moffat, A.E. Lutz, G. Dixon-Lewis, M.D. Smooke, J. Warnatz, G.H. Evans, R.S. Larson, R.E. Mitchell, L.R. Petzold, W.C. Reynolds, M. Caracotsios, W.E. Stewart, P. Glarorg, C. Wang, O. Adigum, W.G. Houf, C.P. Chou, S.F. Miller, *Chemkin Collection, Release 3.7*, Reaction Design. San Diego, CA, 2002.
- [14] N. Peters, in: N. Peters, B. Rogg (Eds.), *Lecture Notes in Physics*, M15, Springer-Verlag, Berlin, 1992, pp. 3–12 (Chapter 1).
- [15] G.P. Smith, D.M. Golden, M. Frenklach, N.W. Moriarty, B. Eiteneer, M. Goldenberg, C.T. Bowman, R.K. Hanson, S. Song, W.C. Gardiner, Jr., V.V. Lissianski, Z. Qin. Available from <http://www.me.berkeley.edu/gri-mech>.
- [16] <http://maeweb.ucsd.edu/~combustion/cermech>.
- [17] I. Glassman, *Combustion*, third ed. Academic Press, San Diego, CA, 1996.
- [18] Y. Ju, H. Guo, K. Maruta, T. Niioka, *Combust. Flame* 113 (4) (1998) 603–614.
- [19] N. Darabiha, C.M. Candel, F.E. Marble, *Combust. Flame* 64 (2) (1986) 203–217.
- [20] Y. Ju, H. Matsumi, K. Takita, G. Masuya, *Combust. Flame* 116 (4) (1999) 580–592.

### Comments

*István Gy. Zsély, Eötvös University, Hungary.* In Fig. 2, in which you presented results, there was a note: “overall uncertainty  $\pm 3\%$ ”. Could you explain this?

*Reply.* The overall  $\pm 3\%$  uncertainty shown in Fig. 2 is estimated and verified by comparing measured species concentration and temperature from the Hencken burner flame with equilibrium calculations. The uncertainties may be caused by calibration procedure, flow controller reading and/or other experimental systematic errors. The uncertainties caused by shot noise are negligible.

mechanism is quite worthwhile. The resulting comparisons, in which the GRI mechanism is best at generally lower temperatures, while the San Diego mechanism is somewhat better at the higher temperatures, is consistent with the fact that flow-reactor results were included in developing the former, but not the latter, which is intended as a relatively small, higher-temperature mechanism. Your data will be useful for future improvements of chemical mechanisms.

*Reply.* The authors appreciate your comments on this work.

*Forman A. Williams, UCSD, USA.* This is excellent work. The approach of measuring over a variety of conditions around those of methane flame extinction and comparing results with predictions of more than one

*V.R. Katta, Innovative Scientific Solutions, USA.* You are using global strain rate for comparing the results of experiments and calculations. This is dangerous in the neighborhood of the extinction limit, especially when

the flame structure is changing. There is a big uncertainty in the extinction-limit strain rates of the chemical models. You need to go to the real extinction limits with each model (not a global strain rate number) to see the differences in the flame structure such as self-propagating or diffusion limited. I don't see any reason why these mechanisms cannot predict such a transition in flame structure.

*Reply.* We agree that flame structures are sensitive to the stretch rate near the extinction-limit and uncertainty exists for estimation of the stretch rate. In our work, we

measure the boundary conditions and use the same boundary conditions for the calculations. The global strain rate expression is based on the boundary conditions and is the same for both the experiments and calculations. The local strain rate at the flame will differ from the global strain rate. Unfortunately we did not measure the local strain rate at the flame. However, by using the same boundary conditions, we can assess whether the model properly predicts the transition from a self-propagating flame to a diffusion-limited flame when using the same boundary conditions and its corresponding global strain rate.